MSFC-275

The ENSO Effect on the Temporal and Spatial Distribution of Global Lightning Activity

THEMIS G. CHRONIS

ORAU/NASA/MSFC

STEVEN J. GOODMAN

NOAA/NESDIS

DAN CECIL

UAH/NSSTC

DENNIS BUECHLER

UAH/NSSTC

JASNA PITTMAN

ORAU/NASA/MSFC

FRANKLIN R. ROBERTSON

NASA / MSFC

RICHARD J. BLAKESLEE

NSSTC/NASA/MSFC

MANUSCRIPT SUBMITTED TO *GEOPHYSICAL RESEARCH LETTERS*

Submitted: June 2007

Corresponding author: Themis Chronis, Oak Ridge Associate Universities / Global Hydrology Climate Center, NASA-Marshall Flight Space Center, 320 Sparkman Dr, Huntsville 35805, AL,

Tel: 256-961-7583. E-mail: chrontx@nsstc.nasa.gov

Abstract

The recently reprocessed (1997-2006) OTD/LIS database is used to investigate the global lightning climatology in response to the ENSO cycle. A linear correlation map between lightning anomalies and ENSO (NINO3.4) identifies areas that generally follow patterns similar to precipitation anomalies. We also observed areas where significant lightning/ENSO correlations are found and are not accompanied of significant precipitation/ENSO correlations. An extreme case of the strong decoupling between lightning and precipitation is observed over the Indonesian peninsula (Sumatra) where positive lightning/NINO3.4 correlations are collocated with negative precipitation/NINO3.4 correlations. Evidence of linear relationships between the spatial extent of thunderstorm distribution and the respective NINO3.4 magnitude are presented for different regions on the Earth. Strong coupling is found over areas remote to the main ENSO axis of influence and both during warm and cold ENSO phases. Most of the resulted relationships agree with the tendencies of precipitation related to ENSO empirical maps or documented teleconnection patterns. Over the Australian continent, opposite behavior in terms of thunderstorm activity is noted for warm ENSO phases with NINO3.4 magnitudes with NINO3.4>+1.08 and 0<NINO3.4<1.08. Finally, we investigate the spatial distribution of areas that consistently portrayed enhanced lightning activity during the main warm/cold (El Niño/La Niña) ENSO episodes of the past decade. The observed patterns show no spatial overlapping and identify areas that in their majority are in agreement with empirical precipitation/ENSO maps. The areas that appear during the warm ENSO phase are found over regions that have been identified as anomalous Hadley circulation ENSO-related patterns. The areas that appear during the cold ENSO phase are found predominantly around the west hemisphere equatorial belt and are in their majority identified by anomalous Walker circulation.

1. Introduction

The El Niño Southern Oscillation (ENSO) is one of the most prominent interannual phenomena. A typical "warm" ENSO phase (El Niño) is depicted through anomalously warm waters, weak easterly trade winds and enhanced precipitation over the equatorial east Pacific, while drier surface conditions are evident over the equatorial west Pacific and the Maritime continent (McPhaden 1999; Rasmussen and Wallace, 1983; Curtis and Adler 2003). Overall anomalies of the opposite sign accompany the "cold" ENSO phase (La Niña). Studies addressing the indirect (teleconnection) ENSO impact mainly focus on the upper mid-latitude (jet stream) circulation, which in turn, affects regional storm track and intensity (Yang et al, 2002, Arkin 1982). The variation of global precipitation distribution has been traditionally the leading diagnostic parameter used to highlight the in situ or teleconnection ENSO-related forcing. Several researchers have documented significant findings between ENSO and precipitation variations; among these we cite: Maritime continent (Curtis and Adler, 2003), India (Rasmusson and Carpenter, 1983), northern South America (Brazil) (Kousky et al 1984), southern Argentina (Grimm et al, 1998), the northern equatorial Atlantic (Enfield and Mayer, 1997; Curtis and Hastenrath, 1995), the United States (Ropelewski and Halpert, 1986) and southeastern China (Gong and Wang, 1999; Wang, 2005). Pioneering work by Ropelewski and Halpert, (1987) (henceforth RH87) have merged the global precipitation distributions with respect to the warm/cold ENSO in a single map of wet/dry surface conditions.

Presence of lightning in clouds signifies charged ice riming particles and super

cooled water droplets in a developing or mature convective environment of strong updrafts (Takahashi et al., 1999; Williams et al., 1993; Blakeslee et al., 1989). Precipitation and electrification are two processes that may coexist in the same cloud-system although they are sensitive and responsive to different environmental factors. Lightning is responsive to microphysical (e.g. ice), kinematic (e.g. vertical motion) as well as thermodynamic (e.g. wet bulb temperature) regimes of precipitating systems (Del Genio and Kovari, 2002; Williams, 1994). Humidity is one the main controlling factors for precipitation. While enhanced condensation can occur in both deep and shallow precipitating systems, enhanced lightning activity is more often found in environments of high vertical development (Williams, 1989). ENSO is known to have an effect on both precipitating as well as dynamic/kinematic regimes (Barnett, 1984; Hsu and Wallace, 1976).

Currently, the Optical Transient Detector (OTD) and the Lightning Imaging Sensor (LIS) provide the most complete coverage of global lightning observations (Christian et al. 2003; Christian et al. 1992; Boccippio et al. 2000; 2002). Unlike precipitation, a very small number of studies have focused on the global lightning/ENSO relationship from a climatological perspective (Satori and Ziegler, 1999). The study at hand employs the recently reprocessed 101 months (12/1997-04/2006) of OTD/LIS database in order to investigate the global distribution of lightning activity as a response to the ENSO variability. The main topics addressed herein are as follows: comparison between the global lightning and precipitation temporal evolution in relation to the ENSO (section 3), ENSO magnitude as a function of the regional extent of thunderstorms (section 4) and the geographical distribution of the areas that showed consistent enhancement of thunderstorm activity during the two major warm (El Niño) and cold (La Niña) ENSO episodes of the past decade (section 5).

2. Data and Methodology

The Optical Transient Detector (OTD) is a space-based instrument specifically designed to detect and locate lightning discharges. This instrument was a scientific payload on the MicroLab-1 satellite that was launched into low Earth orbit in April 1995. Given the trajectory of the satellite, a given regions on the Earth is observed more than 400 times during an 1-year period. The average duration of each observation is approximately 3 minutes. The OTD instrument detects the total lightning activity (Intra Cloud -IC and Cloud to Ground-CG) that occurs within its 1300 x 1300 km^2 field of view (FOV) during both day and night. The Lightning Imaging Sensor (LIS) also monitors the IC and CG, occurring within 80 seconds from the storm's passing through the sensor 600 x 600 km^2 FOV. LIS is part of the Tropical Rainfall Measuring Mission (TRMM) launched in December 1997. Although LIS provides coverage within a 35°S-35°N-latitude zone, its sampling frequency is limited to roughly one overpass per day for any given geographical location.

The diagnostic variable used in the study is the Low Resolution Time Monthly Series (LRTMS) OTD/LIS combined flash rate. This product has undergone temporal and spatial averaging in order to account for the different orbital altitudes of the sensors (Christian et al. 2003). The 101 months included in this study include the overlapping time window of the two sensors (12/97-04/00) as well as the extended TRMM mission (04/00-04/06). The geographical area examined encompasses only the common viewing area of both sensors (35°S-35°N). Flash rates are mapped in a 2.5x2.5 degrees longitude/latitude grid. The subsequent analysis uses lightning (flash rate) anomalies

(LA) calculated relative to the ~9 year mean for each month. The data analysis does not include any additional explicit storm characteristics (e.g. number or size of storms). Therefore the positive (negative) LA can be physically associated with either increased (decreased) thunderstorm frequency/size and/or increased (decreased) average flash rate over a given area.

Monthly precipitation anomalies (PA) are based on the Climate Prediction Center (CPC) Merged Analysis of Precipitation (CMAP, Xie and Arkin 1997). The CMAP analysis is based on a 2.5x2.5 degree longitude/latitude grid. PA are similarly calculated relative to the ~9 year CMAP mean for each month. Positive (negative) PA does not differentiate whether the anomalies are related to storm frequency/size increase (decrease) and/or overall increased (decreased) precipitation rate over a given area.

Figures 1a and 1b show the climatological spatial distribution for both diagnostic variables used by this study. Figure 1a illustrates the CMAP 101 monthly mean precipitation (mm/h). Figure 1b illustrates the OTD/LIS 101 month combined flash rate (flashes per year per km^2). Precipitation maxima are predominant over the Inter Tropical Convergence Zone (ITCZ) (Fig.1a) while Fig.1b reveals the continental preference that lightning is known to have, with Africa being the lightning-dominant region. The variable employed to quantify the temporal evolution of the ENSO cycle is the NINO3.4. This index is calculated on a monthly basis from Sea Surface Temperature (SST) spatial averages between 5°North-5°South and 170°West-120°West.

3. Temporal Evolution of Lightning and Associated Precipitation Anomalies as a function of the NINO3.4

All the correlations employed in the current and following sections are based on the zero-lag, ranked-sum Spearman method. Figure 2a illustrates temporal correlation map for PA/NINO3.4. Correlations in Fig.2a are calculated between the 101 monthly PA time series with the 101 respective monthly NINO3.4 time series for every grid point of the study area. For the given degrees of freedom (dof=99), statistically significant (99% confidence level) correlations are (absolute) values greater than ~0.3. The areas with significant PA/NINO3.4 temporal correlations (Fig.2a) are located: 1) along the equator where the anomalous Walker cells contribute to the low level divergence over the Maritime continent and northeast South America (Brazil) (Bjerknes, 1969). This is exhibited by the observed negative PA/NINO3.4 correlation values over the aforementioned areas 2) the anomalous low level convergence that forces precipitation enhancement over the equatorial central Pacific (Wang, 2005). This is also depicted (Fig.2a) by the positive PA/NINO3.4 temporal correlation over the aforementioned areas. Studies have extensively shown that ENSO introduces direct interactions with the upper level circulation (e.g. mid-latitude Pacific jet stream), which further affect the precipitation climatology over areas distant from its main axis of influence (Arkin, 1982; Rasmusson and Carpenter 1982; Pan and Oort 1983). Such teleconnection patterns can be also identified from Fig.2a; we observe significant PA/NINO3.4 correlations away from the equator and located over: southern South America (Argentina-positive), east-equatorial African coast (positive), southern Africa (negative), southern United States (positive) and Southwest Pacific (negative).

Figure 2b illustrates the temporal correlation map for LA/NINO3.4. Correlations are calculated between the 101 monthly LA series and the 101 monthly NINO3.4 series for every grid point in the study area. The comparison between Fig.2a and Fig.2b

includes the following cases: a) identify areas where ENSO has an "analogous impact" on both precipitation and lightning variables. In other words, these areas should both have significant and same sign PA/NINO3.4 and LA/NINO3.4 correlations b) Identify environments where lightning is more reactive to ENSO forcing. The opposite scenario is not investigated since the main focus of the study is lightning. These areas should appear with significant LA/NINO3.4 correlations and not significant PA/NINO3.4 correlations c) "decoupling" between lightning and precipitation as a function of ENSO explained variability which addresses areas with significant LA/NINO3.4 and PA/NINO3.4 correlations, but of the opposite sign.

Comparison between Fig.2a and Fig.2b primarily reveal coincident observations with correlations of the same sign. Coincident positive (negative) correlations reveal precipitation related to "wet" surface conditions and lightning related to enhanced thunderstorm conditions during a warm (cold) ENSO phase. Regions with the above characteristics are observed over: equatorial central equatorial and south west Pacific Ocean; east Maritime continent (Philippines); northeast Australia; southwest Indian Ocean; south Africa; northern South America (Brazil); north Gulf of Mexico; southeast South America (Argentina) and northeast Pacific.

An example where significant LA/NINO3.4 correlations are not accompanied by significant PA/NINO3.4 correlations is noted where (Fig.2a, b) negative LA/NINO3.4 correlations appear to the north and the south of the central equatorial Pacific (east of the dateline) while no accompanied significant PA/NINO3.4 are present. The negative LA/NINO3.4 over the aforementioned areas shows that lightning variability is responsive to the overall suppressed convective environment related to the typical anticyclonic circulation encountered in the east Pacific during the warm ENSO phase (Arkin, 1982). Other areas falling in the same category can be found over: east China, southeast Australian coast, Indian peninsula and southern Mediterranean/northern Africa. Wang (2005) identifies east China and the southern U.S. as centers of low-level anomalous ascending motion, thus environments prone to convection. Over the aforementioned areas Arkin (1982) documents a 200-hPa zonal wind variability that is statistically related to the onset of warm ENSO phase. Along these lines, Goodman et al. (2000) observe a 200% relative increase in lightning activity over the Gulf of Mexico temporally and spatially coincident with the jet level (200-hPa) anomalous flow during the December-February 1997/1998 warm ENSO phase.

Another interesting case addressing a strong precipitation/lightning decoupling is portrayed over the west Maritime continent (Sumatra) (Fig. 2a, b). PA/NINO3.4 correlations indicate "dry" surface conditions while LA/NINO3.4 correlations indicate enhanced thunderstorm activity. Similar observations over parts of the Maritime continent and during the warm ENSO of 1997/1998 are documented by Morimoto et al. (2006). Hamid et al. (2001) discuss that temperature gradient between the ocean neighboring to a-more-responsive-to-heating continent (e.g. Maritime continent) can reflect on enhanced conditional instabilities, updraft strength and overall deeper convective clouds. These conditions, despite the overall warm ENSO phase that forces precipitation depression over the area, may lead to deeper and electrified convective clouds (Williams, 1994; Keenan, 1994).

4. Impact on ENSO magnitude on the spatial extent of global thunderstorm distribution

We use lightning as the main diagnostic variable in order to answer to the following questions: does ENSO magnitude have an effect on the spatial distribution of lightning activity? Would a stronger ENSO produce thunderstorms of greater spatial coverage and where? ENSO effects are known to have different impacts dependent on geographical locations. In addition, lightning has a strong continental preference. For both aforementioned reasons, we apply a 2.5x2.5 degree land/sea mask over: Americas, Africa, southeast Asia, east/west Pacific, Atlantic and Indian Oceans. These areas are further broken down into their respective northern hemisphere (NH, 15°N-35°N), equatorial (EQ, 15°S-15°N) and southern hemisphere (SH, 35°S-15°S) counterparts. Overall these areas represent 21 geographical subsets including Australia.

From the 101-month study period, 50 months exhibited warm (NINO3.4>+0.0) and 50 cold (NINO3.4<+0.0) ENSO phases. A single event returned NINO3.4=0 and is not included in any of the following computations. The 50 warm ENSO months are further broken down into the 10 months around the respective peaks of the two major El Niño (December-March 1997/1998, October 2002-March 2003). These months fall in the NINO3.4>+1.08 range ("stronger" warm ENSO phase). The remaining 40 months fall in the +0.00<NINO3.4<+1.08 range ("weaker" warm ENSO phase).

For each of the 21 geographical regions we count the number of grid points that have LA>0 and divide it by the total number of grid points that represent the associated region (PLA). PLA quantifies the percent of the geographical subset area that is associated with enhanced thunderstorm activity. For all 21 areas, correlation values are computed between the monthly PLA series and their respective NINO3.4 monthly magnitude. Table 1 reports the correlation values (ρ) that are significant in the 99% confidence level (dof=38, dof=8 and dof=48). Positive ρ sign in the warm phase relates to increasing PLA with increasing positive NINO3.4. The negative ρ sign in the warm phase relates to decreasing PLA with increasing positive NINO3.4. The positive ρ sign in the cold phase relates to decreasing PLA with increasing negative NINO3.4. Finally the negative ρ sign in the cold phase relates to increasing of PLA with increasing negative NINO3.4. The "*ns*" stands for "non significant correlation", at the 99% confidence level.

Four selected cases from Table 1 are presented in a scatter plot (Figs.3a-d). These include SH Africa, EQ Atlantic, NH Southeast Asia and Australia. Each of the Figs.3a-d consists of two panels. The left panel highlights the geographical subsets (dotted regions) over which the respective PLA/NINO3.4 correlations are computed. The right panel illustrates the main scatter plot between the PLA/NINO3.4 values. Gray crosses indicate the 10 months of the "stronger" warm ENSO phase (Fig.3a, c, d). Black crosses indicate either the 40 months of the "weaker" warm ENSO phase (Fig.3a, c, d) or the 50 months of the cold ENSO phase (Fig.3b). In Fig.3a, we plot SH Africa 40-month warm ENSO phase relationship for PLA/NINO3.4 (black crosses, ρ="*ns*"-Table 1) as well as the 10-month warm ENSO phase relationship also for PLA/NINO3.4 (gray crosses, ρ=-0.95-Table 1). In Fig.3b, we plot EQ Atlantic *50*-month cold ENSO phase relationship for PLA/NINO3.4 (black crosses, ρ=+0.72-Table 1). In Fig.3c, we plot *NH* southeast Asia 40-month warm ENSO phase relationship for PLA/NINO3.4 (black crosses, ρ=+0.61-Table 1) as well as the 10-month warm ENSO phase relationship also for PLA/NINO3.4 (gray crosses, ρ="ns"-Table 1). In Fig.3d, we plot Australia 40 month warm ENSO phase relationship for PLA/NINO3.4 (black crosses, ρ=-0.45-Table 1) as well as the 10-month warm ENSO relationship also for PLA/NINO3.4 (gray crosses, ρ=+0.93-Table 1).

Although the above approach does not attempt to isolate seasonally evolving

ENSO characteristics (e.g. boreal summer ENSO vs. boreal winter ENSO) or possible lagged ENSO-related responses (Enfield and Mayer, 1997), it does highlight that the majority of the areas in Table 1 have respective correlations and reveal consistent characteristics with Fig.2b as well as with other ENSO existing literature. Examples that portray these cases are:

-EQ Africa, where we observe enhanced positive PLA/NINO3.4 relationship-Table1, positive LA/NINO3.4 correlation-Fig.2b and precipitation enhancement during warm ENSO phase-RH87)

-EQ Americas: here we observe negative PLA/NINO3.4 relationship-Table1, negative LA/NINO3.4 correlation-Fig.2b and enhanced precipitation during cold ENSO phase-RH87; Kousky et al 1984)

-SH Africa: we observe negative LA/NINO3.4 correlations-Fig.2b, negative PLA/NINO3.4 relationship-Table1/Fig.3a and enhanced precipitation during cold ENSO phase-RH87); Mason and Jury (1997) also document enhanced precipitation during the cold ENSO phase.

- NH east Pacific: we observe a decreasing PLA relative to an intensifying cold ENSO phase-Table 1 and positive LA/NINO3.4-Fig.2b. This area does not show up in RH87 but earlier findings agree with the fact that, over the NH east Pacific, a cold ENSO phase contributes to increased vertical wind shear and overall decreased storm activity (Arkin, 1982).

-EQ Atlantic: this region shows strong linearity describing an increasing PLA during intensification of cold ENSO phases (Table 1 and Fig.3b) while an also significant correlation (of lesser magnitude) for the warm ENSO phase. Significant correlation coefficients are observed in Fig.2b. Atlantic basin teleconnections have been the focus of numerous studies (Enfield and Mayer, 1997; Wang 2005). In accordance with our findings from Table 1, Dong et al. (2000) report that the tropical Atlantic region is related to storm enhancement during both 1998/1999 (cold) and 1997-1998 (warm) ENSO phases.

-NH southeast Asia: Table 1 and Fig.3c reveal a positive PLA/NINO3.4 linear relationship for the "weaker warm ENSO phases" while a positive LA/NINO3.4 is also corroborated in Fig.2b. Wang et al (2000) document warmer and moister conditions over the East Asian coast during a warm ENSO phase. In section 5 we underline that part of this region is associated with one of the "usual suspects" that show up as consistently enhanced lightning activity during warm ENSO phases.

Further remarks pertaining to Table 1/Fig.3 are as follows: all areas reported with significant correlations do not consist of the main ENSO axis of influence, such as EQ east-central (dateline) Pacific and/or EQ Maritime continent. Furthermore, the only common geographical region that appears with significant PLA/NINO3.4 correlations in both stronger and weaker warm ENSO phases is Australia (Table 1/Fig.3d). More precisely, a negative PLA/NINO3.4 relationship is observed during the "weaker" warm ENSO phase and a positive PLA/NINO3.4 during the "stronger" warm ENSO phase. Morimoto et al. (2001) corroborate the previous results by reporting enhanced lightning activity (LA>0) over Australia during the 1997/1998 warm ENSO phase. Benoit and Delcroix (2000) document a similar linear relationship (weaker warm ENSO phase), between observed precipitation and ENSO magnitude over New Caledonia. Australia is one of the regions that RH87 have also identified as "dry" surface conditions during the

warm ENSO phase. Under the same umbrella we cite the case of NH west Pacific where, Wang and Chan (2002) also documented an overall decrease of storm activity during the warm ENSO phase. Whether this two inconsistencies (Australia and NH west Pacific) are exclusive characteristics of the two major warm ENSO phases need further analysis. Similar changes in the dynamics of the ENSO cycle are documented between a weak warm and a strong ENSO phase. As an example we cite the work by Rasmusson and Wallace (1983) who report intensification of the mid-latitude Jet circulation to the East during the transition to the El Nino conditions. From our analysis, an observation that could be linked to the aforementioned is the eastward shifting of PLA/NINO3.4 significant correlations between NH southeast Asia (weaker warm ENSO phase-Table 1) and NH west Pacific (stronger warm ENSO phase-Table 1).

Although the analysis implemented in this section does not address the question of whether a warm/cold ENSO phase would affect regional flash rate and/or size and/or thunderstorm frequency, we have found strong indications of linear relationships between observations of enhanced lightning activity and the respective NINO3.4 magnitude. These findings do not provide a physical basis to infer cause and effect, because of both the nature of the correlation coefficient itself as well as the arbitrary selection of the geographical regions. Although they do provide a diagnostic approach that reveals that over the previously highlighted geographical areas (e.g. SH Africa, EQ Atlantic, Australia etc.) NINO3.4 magnitude (hence SST anomalies along the EQ Pacific) is related to the regional extent of thunderstorm distribution. Meridional and zonal ENSO-related heat transport has identified areas, which their regional atmospheric circulation is affected (Wang et al. 2000; Wang, 2005). The mechanisms that lead to the observed linear response of thunderstorm regimes over certain regions will be further investigated by ingesting additional thunderstorm characteristics (e.g. TRMM attributes).

5. Consistent Spatial Patterns of positive LA during ENSO phases

Consistent occurrence of LA>0 over certain areas during ENSO phases of a given NINO3.4 magnitude or greater (in absolute terms), can be indicative of repetitive patterns of enhanced regional thunderstorm activity. In order to investigate the areas over which such patterns occur, we put forward the following analysis. Figure 4 highlights the areas that consistently yielded LA>0 for all NINO3.4>+1.08 and the areas that consistently yielded LA>0 for all NINO3.4<-1.22. This scenario involves the 10 months around the respective peaks of the two major El Niño (December-March 1997/1998, October 2002-March 2003) and the 10 months around the respective peaks of the two major La Niña (October 1998-February 1999 and November 1999-March 2000). Red (blue) contours outline the adjacent areas of LA>0 during a warm (cold) ENSO phase. This analysis differs from the method followed in section 4 in that, we focus over areas with consistent LA>0 instead of individual counting of LA>0 observations. The fact that we are focusing in the displayed adjacent areas (red-blue contours - Fig.4) is because these may identify (convective) areas of mesoscale weather patterns during a warm/cold ENSO phase.

A key observation from Figure 4 is that no overlapping areas with LA>0 are noted; this fact may serve as an indication that lightning shows strong regional preference during different ENSO phases. Areas related to the warm ENSO phase are mostly located away from the equator and have been identified by numerous researchers as regions of anomalous jet stream circulation (Gulf of Mexico, east China and southeastern South America-red contours, Arkin, 1982; Wang, 2005; Ropelewski and Halpert, 1986). These regions along with Sumatra also appeared as areas of strong positive LA/NINO3.4

correlation values (Fig.2b). In particular, the case of east China has been consistently appearing as 1) an area that shows strong temporal correlation with NINO3.4 (Fig.2b) 2) a part of a greater area, where thunderstorm extent shows positive trend with the NINO3.4 magnitude (Table 1/Fig.3c) 3) an area that has consistently enhanced thunderstorm activity during the two major warm ENSO phases (Fig.4-red contour).

The areas of cold ENSO phase are found to be more equatorward. Among these, the most extensive areas are observed over the tropical Atlantic, central/south Africa, southwest and northeast South America and the Philippines. The tropical Atlantic is among the geographical regions that have received a great deal of debate regarding its teleconnection relationship to ENSO (Enfield and Mayer, 1997). As in the previous case of east China, the tropical Atlantic shows 1) an area that exhibits strong temporal correlation with NINO3.4 (Fig.2b) 2) a part of a greater area, where thunderstorm extent shows positive trend with the NINO3.4 magnitude (Table 1/Fig.3c) and 3) an area that has consistently enhanced thunderstorm activity during the two major cold ENSO phases (Fig.4-blue contour). Consistent with our findings, Wang (2005) identifies an anomalous air descent over the tropical Atlantic (suppressed storm activity). In the same category we also include the eastern EQ South America (Brazil). Wang et al. (2000) identifies the anticyclone over Sea of Philippines as a major characteristic of the anomalous ENSO-related circulation over the northeast Hemisphere.

Although this study and RH87 follow different analysis paths, they reveal worth noting similarities; these are found during the warm ENSO (red contour) phase mainly over Gulf of Mexico, Indian Ocean and southeast South America (Argentina) during the cold ENSO phase (blue contour) over northeast South America (Brazil) and the Philippines. Both the east China (red contour, not shown in RH87) and the Philippines (blue contour) are both coincident with the area of enhanced precipitation and anticyclonic circulation accordingly, both related to the warming along the equatorial Pacific (Wang et al. 2000). The western Maritime continent (Sumatra, red contour-Fig.4) case discussed in section 3 shows up again to have characteristics of sustained thunderstorm activity (LA>0).

6. Conclusions

Despite the uncertainties related to the precipitation retrieval methods of the modern era (mainly by satellites carrying microwave sensors), that eventually appear as discrepancies in the global ENSO-related precipitation distribution (Soden, 2000; Spencer, 1993), the mechanisms that link the ENSO/precipitation patterns have been studied broadly by many investigators. On the contrary, the absence of historical global lightning observations has hampered global ENSO-lightning related studies. The significance of this study lies in the fact that it is the first to use historical global lightning data to infer ENSO-related regimes. We have identified areas over which the temporal ENSO variability explains some of the global patterns of lightning activity. Most of these areas are found to agree in terms of the spatial precipitation distribution and the typical signatures of the ENSO/Walker circulation. Areas where lightning/NINO3.4 correlations are significant and precipitation/NINO3.4 correlations are not significant are found over both hemispheres (e.g. Gulf of Mexico, southeast South America, north/south Indian Ocean, east China/east Australian coast). Existing ENSO literature identifies them as ENSO-related upper level anomalous circulation. A special case is observed over the western Maritime continent where typical drought conditions during a warm ENSO phase are related to highly explained lightning activity in terms of ENSO variability.

Significant findings that relate the spatial thunderstorm extent as a function of the NINO3.4 magnitude are presented. The majority of these cases are consistent with spatial distribution of the wet/dry surface conditions that are traditionally related to the documented ENSO effects. For the case of the Australian continent, the observed contradicting behavior of thunderstorm spatial extent between the stronger and weaker warm ENSO phases will be further studied. The findings of section 4, add a valuable insight to the current "binary" wet/dry surface conditions that RH87 offers. The observed linear response between thunderstorm extent and the ENSO magnitude needs further investigation in order to examine any relationships between explicit local forcings (e.g. vertical wind shear) and the regional thunderstorm extent. Furthermore, we have studied persistent spatial patterns of enhanced lightning activity during the two major warm and cold ENSO phases included in the study period (1997-2006). We have identified areas that have been consistency related to enhanced thunderstorm activity (LA>0) during the strongest warm (December-March 1997/1998, October 2002-March 2003) and strongest cold (October 1998-February 1999 and November 1999-March 2000) ENSO phases of the past decade. Interestingly, no overlapping areas are observed, underlining that lightning shows strong regional preference between the two ENSO phases. The observed areas related to the warm ENSO phase are mainly found in the NH hemisphere, and over regions where teleconnection ENSO related effects have been documented. The observed areas during the cold ENSO phase are mainly found along the equatorial Atlantic and western coast of South America. The combined observations from sections 4 and 5 can be used as validation or external forcings in climatological models used to simulate the ENSO evolution.

Ongoing efforts include the reprocessing of other TRMM-related thunderstorm climatological features in order to further study whether ENSO magnitudes do have exclusive impact on regional flash-rate and/or thunderstorm frequency/size. Future continuous global lightning monitoring can contribute to the deeper understanding of planetary scale phenomena such as the ENSO (Christian et al., 1989).

Acknowledgments

The TRMM scientific team provides the OTD/LIS dataset. This can be downloaded at http://thunder.nsstc.nasa.gov/data/. The first author would like to extent a sincere thanks to Dr. Ramesh Kakar for the awarded NASA post-doctoral fellowship. The first author also acknowledges the contribution of the Oak Ridge Associated Universities. We would also like to thank Dr. David Fanning for the helpful suggestions in the IDL programming.

References

Arkin, P.A., The relationship between interannual variability in the 200mb tropical wind field and the Southern Oscillation, *Mon. Wea. Rev.*, 110, 1393-1404), 1982.

Barnett, T.P., Interaction of the monsoon and Pacific trade wind system at interannual time scales. Par III: A partial anatomy of the Southern Oscillation. Mon. Wea. Rev., 112, 2388-2400, 1984.

Benoit, J., and Delcroix, T., ENSO-related precipitation changes in New Caledonia, Southwestern tropical Pacific, Mon. Wea. Rev., Vol.128, pp.3001-3006, 2000

Bjerkens, J., Atmospheric teleconnections from the equatorial Pacific, Mon. Wea. Rev., 97, 163-172, 1969.

Blakeslee, R. J., H. J. Christian, and B. Vonnegut, Electrical measurements over

thunderstorms, J. Geophys. Res., 94 (D11), 13135-13140, 1989.
Boccippio, DJ; Koshak, WJ; Blakeslee, R.J., Performance assessment of the Optical Transient Detector and Lightning Imaging Sensor: I. Predicted diurnal variability. J. Atmos. Oc. Tech. 19, 1318-1332, 2002.

Boccippio,D.J., Driscoll,K.T., Koshak,W.J., Blakeslee,R.J., Boeck,W.L,, Mach,D.A., Buechler,D.E,, Christian,H.J., Goodman,S..J., The Optical Transient Detector (OTD): Instrument characteristics and cross-sensor validation. J. Atmos. Oc. Tech. 17, 441-458, 2000.

Christian, H. J., R. J. Blakeslee, and S. J. Goodman, The detection of lightning from geostationary orbit, J. Geophys. Res., 94(D11), 13329-13337, 1989

Christian, H. J., R. J. Blakeslee, D. J. Boccippio, W. L. Boeck, D. E. Buechler, K. T. Driscoll, S. J. Goodman, J. M. Hall, W. J. Koshak, D. M. Mach, and M. F. Stewart, Global frequency and distribution of lightning as observed from space by the Optical Transient Detector, J. Geophys. Res., 108 (D1), 4005, 10.1029/2002JD002347, 2003.

Christian, H.J., R.J. Blakeslee, and S.J. Goodman, Lightning Imaging Sensor (LIS) for the Earth Observing System, NASA Technical Memorandum 4350, MSFC, Huntsville, AL, February, 1992.

Curtis S., and R. F. Adler, Evolution of El Niño-precipitation relationships from satellites and gauges, J. Geophys. Res., 108 (D4), 4153, 2003.

Curtis, S., and S. Hastenrath, Forcing of anomalous sea surface temperature evolution in the tropical Atlantic during Pacific warm events. J. Geophys. Res., 100, 15835-15847, 1995.

Del Genio, A. D., and W. Kovari, Climatic properties of tropical precipitation convection under varying environmental conditions. J. Climate, 15, 2597-2615, 2002.

Dong, W.B., R.T. Sutton, S.P. Jewson, A. O'Neil and J. M. Slingo, Predictable winter climate in the North Atlantic sector during the 1997-1999 ENSO cycle, Geophys. Res. Lett. Vol. 27, NO. 7, pp 985-988, 2000.

Enfield, D.B., and D.A. Mayer, Tropical Atlantic Sea surface temperature variability and its relation to the El Niño-Southern Oscillation. J. Geophys. Res., 102, 929-945, 1997.

Gong, D.Y., and S.W. Wang, Impacts of ENSO on rainfall of global land and China, Chin. Sci. Bull., 44, 852-857, 1999.

Goodman S. J., D. E. Buechler, K. Knupp, K. Driscoll, and E. W. McCaul Jr., The 1997-98 El Niño event and related wintertime lightning variations in the Southeastern United States, Geophys. Res. Lett., 27(4), 541-544, 2000.

Grimm, A.M., S.E.T. Ferraz, nd J. Gomes, Precipitation anomalies in southern Brazil associated with El Nino and La Nina events, J. Climate, 11, 2863-2880, 1998

Hamid E.Y., Z. Kawasaki, and R. Mardiana, Impact of the 1997-1998 El Niño event on lightning activity over Indonesia, Geophys. Res. Lett., 28(1), 147-150, 2001.

Hsu, C.F., and J.M. Wallace, The global distribution of the annual and asemi-annual cycles in precipitation. Mon. Wea. Rev., 104, 1093-1101, 1976.

Keenan, D. T., B. Ferrier and J. Simpson, Development and structure of a maritime continent thunderstorm, J. of Meteo. Atmosph. Physics, Vol 53, pp 185-222, 1994

Kousky, V.E., M.T. Kagano and I.F.A. Cavalcanti, A review of the Southern Oscillation: oceanic-atmospheric circulation changes and related rainfall anomalies. Tellus, 36A, 490-502, 1984.

Mason, S.J., and M.R. Jury, Climatic variability and change over southern Africa: A reflection on underlying processes. Progr. Phys. Geogr., 21, 23-50, 1997

McPhadden M.J., Climate Oscillations-genesis and evolution of the 1997-1998 El Niño, Science 283: 950-954, 1999

Morimoto, T., ENSO and convective activities by TRMM observations, 2006, LIS International Workshop, Huntsville, AL, 2006.

Pan, Y.H., and A.H. Oort, Global climate variations connected with sea surface temperature anomalies in the eastern equatorial Pacific Ocean for the 1958-73 period. Mon. Wea. Rev., 111, 1244-1258, 1983.

Rasmussen, M., and J. M. Wallace, E., Meteorological aspects the of EI Niño-Southern Oscillation, Science, 222, 1195-1202, 1983.

Rasmussen, M., and T. H. Carpenter, E., The relationship between eastern equatorial Pacific sea surface temperature and rainfall over India and Sri Lanka, Mon. Weather Rev., 517-528, 1983.

Rasmussen, M., and T. H. Carpenter, E., Variations in tropical sea surface temperature and surface wind fields associated with the Southern Oscillation/El Niño, Mon. Weather Rev., 110,354-384, 1982.

Ropelewski, C.F, and M.S. Halpert, Global and regional scale precipitation patterns associated with the AL Niño /Southern Oscillation, Mon. Wea. Rev. 115, 1606-1626, 1987.

Ropelewski, C.F, and M.S. Halpert, North American precipitation and temperature patterns associated with the El Niño Southern Oscillation (ENSO), Mon. Wea. Rev., 114, 2352-2362, 1986

Satori, G., Zieger, B., El Niño related meridional oscillation of global lightning activity, Geoph. Research Letters, Vol. 26, NO. 10, pp 1365-1368, 1999

Soden, B.J., The sensitivity of the tropical hydrologic cycle to ENSO, J. Climate, 13, 538-549, 2000.

Spencer, R.W., Global oceanic precipitation from the MSU during the 1979-91 and comparisons to other climatologies, J. Climate, 6, 1301-1326, 1993.

Takahashi, T., T. Tajiri, and Y. Sonoi, Charges on graupel and snow crystals and the electrical; structure of winter thunderstorms, J. Atmos. Sci., 56, 1561-1578, 1999

Wang, C., ENSO, Atlantic climate variability and the Walker and Hadley circulations, The Hadley Circulation, Past and Future, pp. 173-202, Kluwer Academic Publishers, 2005.

Wang, B., and J.C.L. Chan, How Strong ENSO Events Affect Tropical Storm Activity over the Western North Pacific. *J. Climate*, **15**, 1643–1658, 2002.

Wang, B., Wu, E.R., and Fu, X., Pacific-East Asian teleconnection: How does ENSO affect East Asian climate? J. of Climate Vol. 13, pp. 1517-1536, 2000

Williams, E.R., Global circuit response to seasonal variations in global surface air temperature, Mon. Wea. Rev., 122, 1917-1929, 1994

Williams, E.R., M.E. Weber, and R.E. Orville, The relationship between lightning type and convective state of thunderclouds, J. Geophys. Res., 94, 13,213-13,220, 1989

Williams, E.R., R. Zhang and D.J. Boccippio, The microphysical growth state of ice particles and the large scale electrical structure of clouds. J. Geophys. Res., 99, 10787-10792, 1993

Xie, P., and P.A. Arkin, Global Precipitation: A 17-Year Monthly Analysis Based on Gauge Observations, Satellite Estimates, and Numerical Model Outputs. *Bull. Amer. Meteor. Soc.*, 78, 2539—2558, 1997.

Yang, S., K.M. Lau., K.M. Kim, Variations of the East Asian jet stream and Asian-Pacific-American winter climate anomalies, J. Clim., Vol 15, pp 306-325, 2002

Tables

Table 1. Spearman correlation (ρ) between the PLA and NINO3.4 magnitudes for 50 warm and 50 cold ENSO phases.

Geographical Subsets	*ρ values for PLA/NINO3.4 for 40 months of warm (+0.00<NINO3.4 <+1.08) ENSO phase*	*ρ values for PLA/NINO3.4 for 10 months of warm (NINO3.4>+1.08) ENSO phase*	*ρ values for PLA/NINO3.4 for 50 months of cold (NINO3.4<0.00) ENSO phase*
NH South-East Asia	*+0.61*	*-ns-*	*-ns-*
Australia	*-0.45*	*+0.93*	*-ns-*
EQ Africa	*+0.58*	*-ns-*	*-ns-*
NH West Pacific	*-ns-*	*+0.90*	*-ns-*
NH East Pacific	*-ns-*	*-ns-*	*+0.66*
SH Africa	*-ns-*	*-0.95*	*-ns-*
EQ Americas	*-ns-*	*-ns-*	*-0.47*
EQ Atlantic	*+0.33*	*-ns-*	*+0.72*

Figures

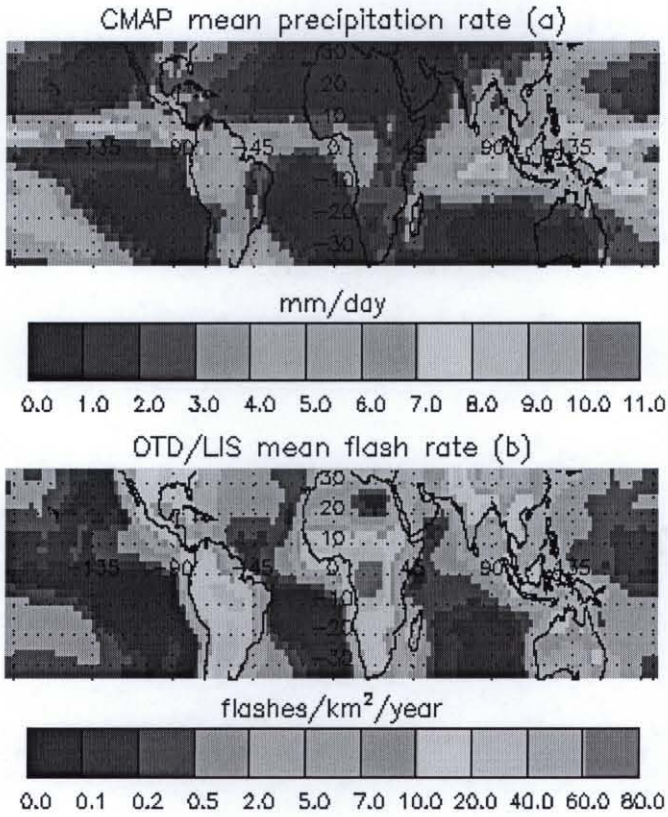

Figure 1a. CMAP mean precipitation rate (mm/h) for the study period (12/97-04/06).

Figure 1b. Global OTD/LIS lightning flash rate (flashes per km^2 per year) for the study period (12/97-04/06).

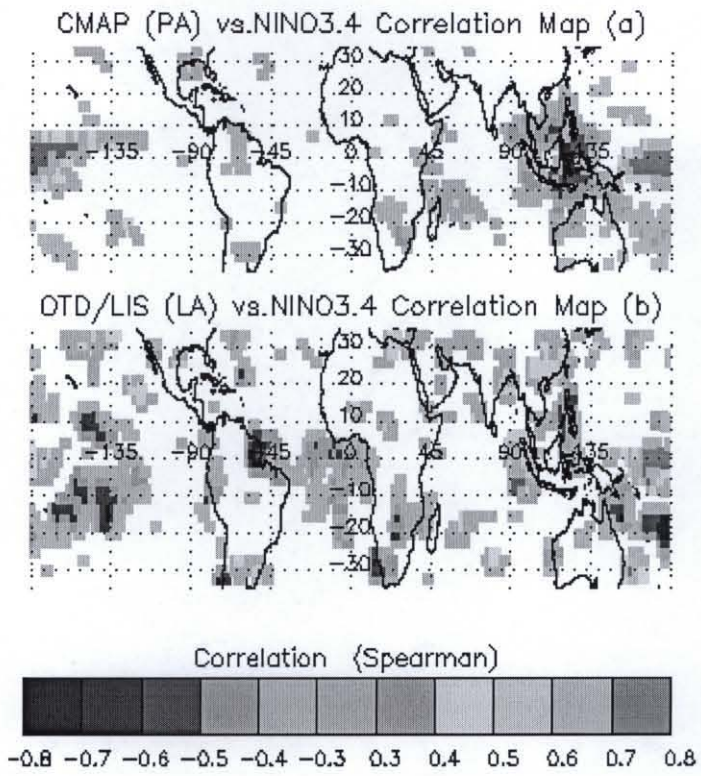

Figure 2a: Temporal correlation map for every grid point between monthly NINO3.4 and monthly (CMAP) PA. The study period is 101 months (12/97-04/06).

Figure 2b: Temporal correlation map for every grid point between monthly NINO3.4 and monthly (LIS/OTD) LA time series. The study period is 101 months (12/97-04/06).

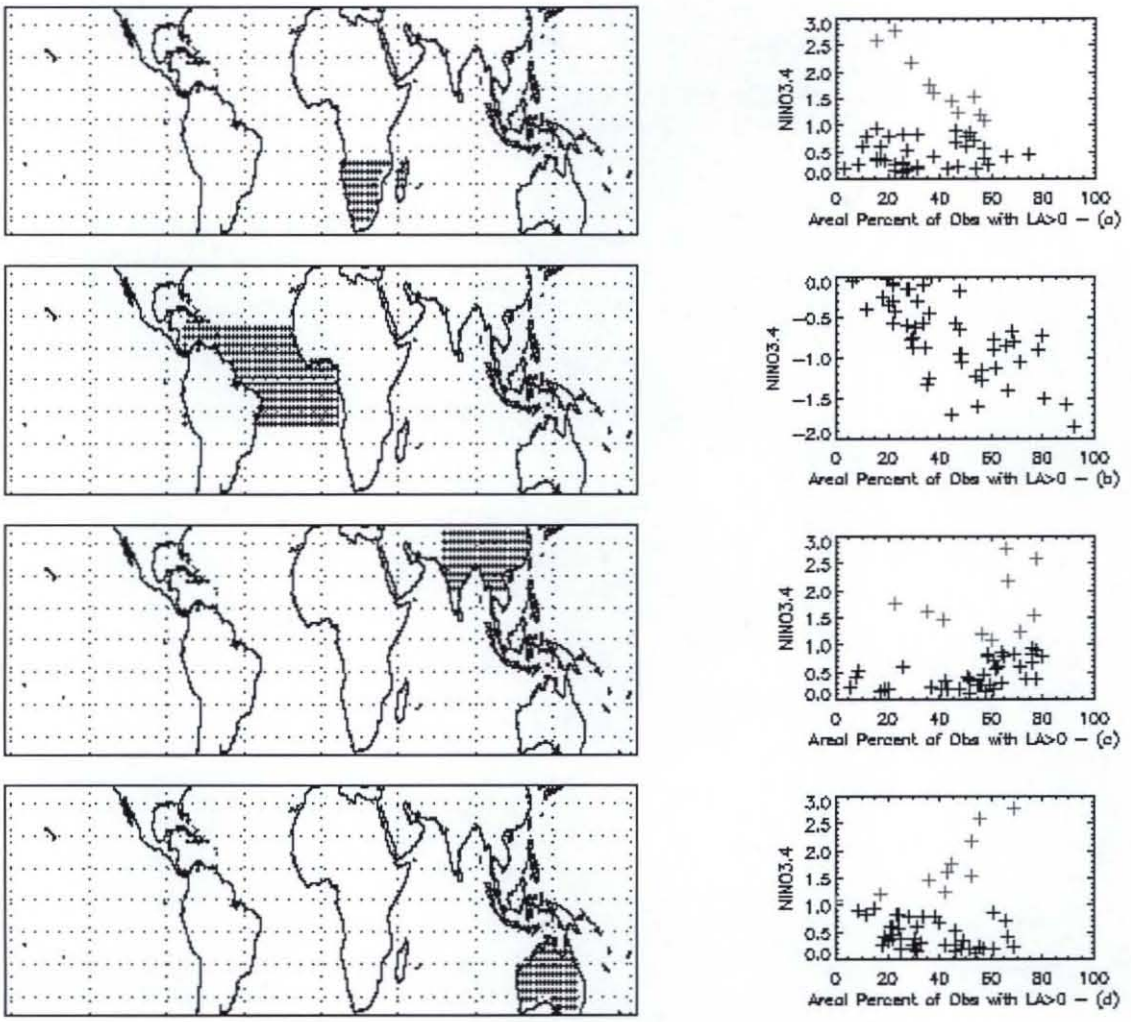

Figure 3. Each of the Figs.3a-d consists of two panels. The left panel highlights the geographical subsets (dotted regions) over which the respective PLA/NINO3.4 correlations are computed. The right panel illustrates the main scatter plot between the PLA/NINO3.4 values. Gray crosses indicate the 10 months of the "stronger" warm ENSO phase (Fig.3a, c, d). Black crosses indicate either the 40 months of the "weaker" warm ENSO phase (Fig.3a, c, d) or the 50 months of the cold ENSO phase (Fig.3b). Fig.3a: SH Africa 40-month warm ENSO phase relationship for PLA/NINO3.4 (black crosses, ρ="*ns*"-Table 1) as well as the 10-month warm ENSO phase relationship also for PLA/NINO3.4 (gray crosses, ρ=-0.95-Table 1). Fig.3b: EQ Atlantic *50*-month cold ENSO phase relationship for PLA/NINO3.4 (black crosses, ρ=+0.72-Table 1). Fig.3c: *NH* southeast Asia 40-month warm ENSO phase relationship for PLA/NINO3.4 (black crosses, ρ=+0.61-Table 1) as well as the 10-month warm ENSO relationship also for PLA/NINO3.4 (gray crosses, ρ="ns"-Table 1). Fig.3d: Australia 40-month warm ENSO phase relationship for PLA/NINO3.4 (black crosses, ρ=-0.45-Table 1) as well as the 10-month warm ENSO phase relationship also for PLA/NINO3.4 (gray crosses, ρ=+0.93-Table 1).

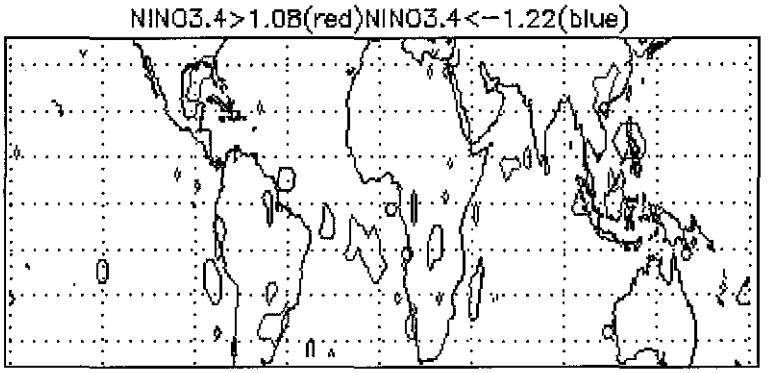

Figure 4. Contours indicate areas with enhanced thunderstorm activity (LA>0) during 10 months around the peak of the two major El Niño (red-December-March 1997/1998, October 2002-March 2003) and 10 months around the peak of the two major La Niña (blue-October 1998-February 1999 and November 1999-March 2000).